NANOSYSTEMS: PHYSICS, CHEMISTRY, MATHEMATICS, 2017, 8 (5), P. 628–634

Two facile routes for functionalization of WS_2 nanotubes with silver nanoparticles

A. Yu. Polyakov[1], V. A. Lebedev[1], L. Yadgarov[2], E. A. Goodilin[1]

[1]Department of Materials Science, Lomonosov Moscow State University, 1-73 Leninskiye gory, Moscow, 119991, Russia

[2]Tel Aviv University, P. O. Box 39040, Tel Aviv 6997801, Israel

a.yu.polyakov@gmail.com, goodilin@gmail.com

PACS 81.10.-h, 88.30.mj **DOI 10.17586/2220-8054-2017-8-5-628-634**

Silver-coated WS_2 nanotubes (NT-WS_2) were successfully synthesized via two wet chemistry techniques. The first employs spontaneous silver nanoparticle growth resulting from an interaction of disulfide nanotubes with $AgNO_3$ in aqueous suspensions at 100 °C without any additional reducing agents or stabilizers. The second utilizes $[Ag(NH_3)_2]OH$ complex to produce silver nanoparticles upon thermal decomposition. Both techniques are capable of producing Ag-NT-WS_2 nanocomposites containing 5–60 nm silver nanoparticles tightly attached to the nanotubes' surfaces. The hexagonal arrangement of sulfur atoms of the outer WS_2 layer was postulated to facilitate crystallization of silver nanocrystals with hexagonal crystallographic system (4H–Ag). The physical-chemical model for spontaneous AgNP formation is proposed.

Keywords: WS_2 nanotubes, silver nanoparticles, plasmonic nanoparticles, nanocomposite, spontaneous growth, 4H silver.

Received: 30 September 2017

Revised: 6 October 2017

1. Introduction

Currently, much attention is paid to the nanocomposites of noble metals and semiconductors due to novel synergistic properties arising in such materials [1]. Among others, semiconducting nanotubes functionalized with silver nanoparticles (AgNPs) were successfully synthesized and became widely studied multifunctional composites. Due to the presence of bright plasmon resonance in Ag nanostructures, such nanocomposites can be employed in numerous optical applications. For example, carbon nanotubes (CNT) coated with Ag and Au nanoparticles have been found to be broad-band optical limiters [2]. Ag-CNT nanocomposites are widely used as mediators for highly-sensitive surface-enhanced Raman spectroscopy (SERS) [3–5]. AgNP-loaded CNT and TiO_2 nanotubes possess high efficiency in photocatalytic applications [6–8] including antibacterial photocatalysis in visible light [9]. Additionally, Ag-CNT nanocomposites are considered promising gas sensors [10, 11], catalysts [12], antibacterial agents [13–15] and drug delivery carriers [16].

WS_2 nanotubes (NT-WS_2) are the analogues of multiwalled CNT and represent folded and nested S-W-S sheets containing six-fold-bonded W atoms sandwiched between three-fold-bonded sulfur atoms [17]. Mass production of NT-WS_2 is based on reduction of WO_3 nanoparticles using a $H_2S/H_2/N_2$ gaseous mixture in fluidized-bed reactors [18]. A number of distinctive advantages of NT-WS_2 were reported. Contrary to CNT, disulfide nanotubes cannot be bent or entangled easily, therefore they are more easily dispersed in polymer blends and other matrices [19]. Individual NT-WS_2's were also shown to be perfect torsional resonators with the highest quality factor (Q) and torsional resonant frequency in comparison to CNT and BN nanotubes [20]. Recently, the unique nonreciprocal superconductive behavior of individual chiral NT-WS_2 was also reported [21]. Surface modification of NT-WS_2 with inorganic nanoparticles expands application areas of disulfide nanotubes. Co@NT-WS_2 [22] and Ni@NT-WS_2 [23] nanocomposites effectively catalyze hydrodesulfurization reactions of thiophene and similar compounds. Additionally, Co@NT-WS_2 is considered as a promising visible-light photocatalyst [24]. Pd@NT-WS_2 nanocomposites were found to be efficient catalysts for cross-coupling (Heck and Suzuki) reactions [25]. $FeWO_4$ nanoparticles were successfully deposited onto NT-WS_2 resulting in magnetic nanocomposites [26]. Recently, CNT/NT-WS_2 electrically conductive hybrid films were also produced [27].

There are plenty of versatile techniques for CNT surface modification, e.g., generation of chemically active carboxylic groups by etching the CNT surface with HNO_3/H_2SO_4 [13, 28]. Similarly, many routes for coating of CNT with AgNPs have been reported, including deposition of pre-synthesized AgNPs [10,11], magnetron sputtering of Ag and high-temperature annealing [3], E-beam coating in vacuum [2], Ag_2O reduction upon sonication in presence of CNT [29] and reduction of Ag(I) ions in aqueous CNT suspensions. The latter includes direct photoreduction, thermal decomposition [8], usage of reducing agents (e.g. glucose [14], formaldehyde [28], etc.)

and sacrificial layers [9], as well as spontaneous reduction of Ag^+ ions on the surface of CNT [30]. On the contrary, the functionalization of NT-WS_2 with plasmonic silver nanoparticles has not been studied yet, despite several attempts having been made to synthesize Au-NT-WS_2 nanocomposites [31–34]. Moreover, it was suggested in our previous work [32], which focused on the functionalization of NT-WS_2 with AuNPs via spontaneous $HAuCl_4$ reduction on the disulfide surface, that the same technique could be applied using $AgNO_3$ solutions for the production of Ag-NT-WS_2 nanocomposites.

Going beyond this suggestion, here, we report two facile techniques for decoration of NT-WS_2 with AgNPs: the first is based on a reaction of $AgNO_3$ with aqueous NT-WS_2 suspension at 100 °C; the second employs the thermal decomposition of freshly prepared $[Ag(NH_3)_2]OH$ complex solution in the presence of disulfide nanotubes. The resultant nanocomposites are carefully characterized using transmission electron microscopy (TEM).

2. Experimental

WS_2 nanotubes were kindly provided by NanoMaterials Ltd. (Israel) and personally by Prof. Reshef Tenne (Weizmann Institute of Science, Israel). The nanotubes are multiwalled, typically 1–20 μm long and 30–150 nm in diameter. Before all the syntheses the nanotubes were deagglomerated by sonication in acetone according to the common procedure [35].

Silver nitrate was of chemically pure (c.p.) grade. Sodium hydroxide standard solution was purchased from Merck (Germany). All other chemicals were purchased locally and were of analytical grade. All aqueous solutions and suspensions were prepared using high purity water (Milli-Q RG, 18.2 MΩ·cm resistivity, Millipore). Glassware and magnetic stirring bars utilized for AgNP synthesis were washed by 63 % HNO_3.

Within the first technique towards Ag-NT-WS_2 nanocomposites, 14 ml of 114 mM $AgNO_3$ solution were heated up to 100 °C in a foil-wrapped beaker to avoid photoinduced silver salt decomposition. Then, 2 ml of freshly prepared aqueous nanotube suspension (1.3 g/L NT-WS_2) were added to the beaker upon vigorous stirring. The reaction mixture was kept at 100 °C for 3 min and then cooled down to room temperature with continued stirring.

For the second NT-WS_2 decoration technique, freshly prepared $[Ag(NH_3)_2]OH$ complex was used. This technique was adopted from the protocol for AgNP-decoration of SiO_2 microspheres reported elsewhere [36]. For the complex preparation, 0.1 M NaOH was added to 10 ml of 0.01 M $AgNO_3$ in a dropwise manner until the end of Ag_2O precipitation. The resulting brown sediment was centrifuged (4000 rpm, 10 min), redispersed in purified water by 1 min sonication and centrifuged again. This washing procedure was repeated three times. The purified sediment was dissolved in 10 % $NH_3{\cdot}H_2O$ to form 15 mM $[Ag(NH_3)_2]OH$ solution, which was stored at 4 °C and used within 30 min after preparation.

For the nanocomposite synthesis, 2 ml of aqueous nanotube suspension (1.3 g/L NT-WS_2) were added to 13.89 ml of purified water pre-heated up to 100 °C under vigorous stirring. Then, 110 μl of freshly prepared 0.015 M $[Ag(NH_3)_2]OH$ solution were added. The reaction mixture was kept in foil-wrapped beaker at 100 °C for 3 min and then cooled down to room temperature. In both procedures, the WS_2 concentration in reaction mixtures after addition of all the reactants was about 0.66 mM and the Ag concentration was about 0.1 mM.

The nanocomposite morphologies were analyzed using a Carl Zeiss Libra 200 MC transmission electron microscope (TEM) operating at 200 kV. Selected-area electron diffraction (SAED) patterns were registered for representative selection of the particles. For TEM analysis the aqueous composite suspensions were dripped on lacey-carbon copper grids (SPI, USA) and dried. Images were processed using open-source Gwyddion software [37] including calculation and processing of Fast Fourier Transforms.

Scanning electron microscopy (SEM) was performed using Carl Zeiss Leo Supra 55 microscope operating at 15 kV in secondary electron imaging (SE2) regime. For SEM analysis, the composite nanoparticle suspensions were dried on conductive silicon wafers.

3. Results and discussion

The silver-decorated nanotubes were multiwalled, 1–20 μm long and 30–150 nm in diameter. Both developed techniques resulted in functionalization of the NT-WS_2 sidewalls with a layer of silver nanoparticles (Fig. 1,2). If using $AgNO_3$, the size of the nanoparticles varied from 5 nm to 60 nm; the mean size is 30±8 nm (Fig. 1(a-d)). A synthesis with the same concentration of $[Ag(NH_3)_2]OH$ resulted in smaller nanoparticles: from 5 to 35 nm, the mean size being 20±5 nm. As visualized by TEM, in both the cases the nanoparticles are uniformly distributed on the nanotube surface. A few AgNP agglomerates were also detected, especially near the tips of NT-WS_2. The AgNPs covering prepared from $[Ag(NH_3)_2]OH$ looks more uniform and less agglomerated in comparison with those prepared at the same concentration of $AgNO_3$. SEM also revealed patterning of AgNPs along the surface defects of disulfide (Fig. 1(c)). This suggestion is supported by AgNPs deposition on step defects of outer WS_2 layers observed by HRTEM (Fig. 1(d)). The same behavior was previously observed for gold nanoparticles grown on NT-WS_2[32]. The local composition of the Ag-NT-WS_2 nanocomposite prepared using $AgNO_3$ was also visualized using STEM-EDX mapping (Fig. 2). The AgNPs have a characteristic non-spherical shape indicating their heterogeneous nucleation and growth directly on the NT-WS_2 surface. Such growth results in a tight contact between AgNP and disulfide. Free AgNPs detached from nanotube surface or formed in bulk solution are rare.

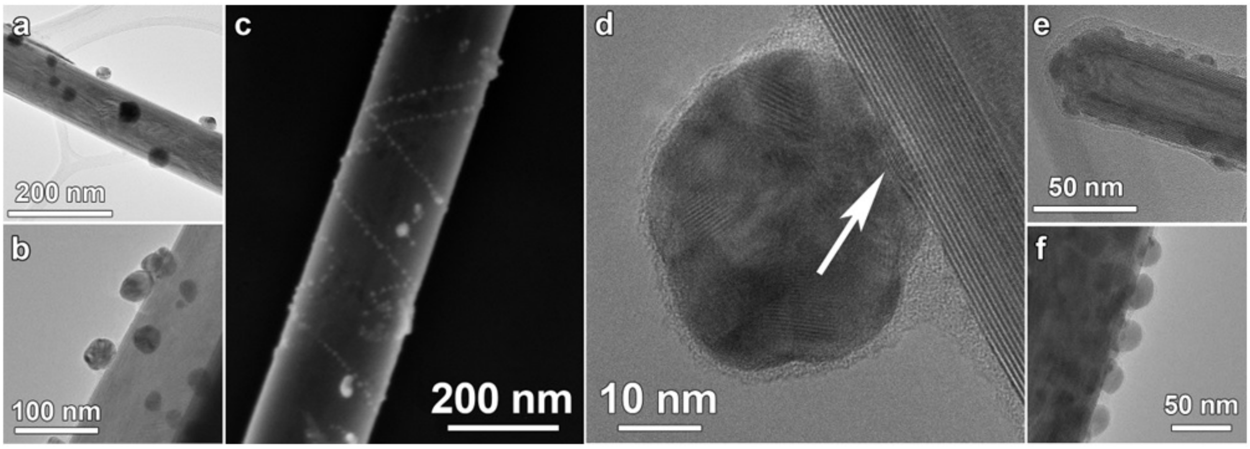

FIG. 1. Micrographs of Ag-NT-WS_2 nanocomposites synthesized using $AgNO_3$ (a-d) and $[Au(NH_3)_2]OH$ (e, f) precursors. The arrow on (d) designates the step defect of NT-WS_2 surface underlying the grown AgNP

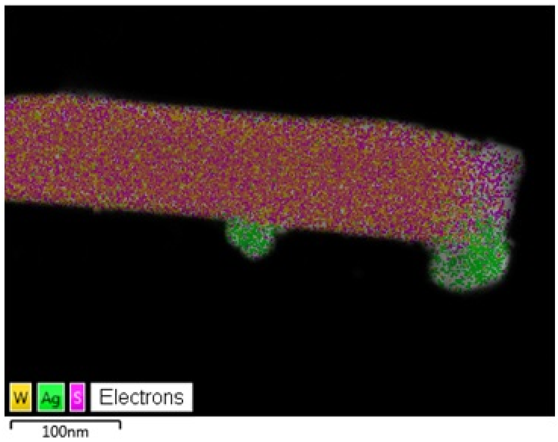

FIG. 2. STEM-EDX mapping of Ag-NT-WS_2 nanocomposite synthesized employing the $AgNO_3$ precursor

HRTEM analysis revealed that, while some grown particles exhibits "normal" (111) and (200) cubic silver (3C-Ag) plane arrays (Fig. 3(a)) with ca. 2.36 Å and ca. 2.00 Å spacings, respectively (Fig. 3(a-c)), the other particles have an unusual hexagonal (4H-Ag) structure. Distinct plane arrays with ca. 2.48 Å spacing were detected (Fig. 3(d-e)), coinciding well with 2.5 Å spacing of (004)-(100) 4H-Ag planes (entry #41–1402, ICDD PDF2 database [38]). To illustrate the difference in nanoparticle structures, Fast Fourier Transforms (FFTs) were calculated from HRTEM images of the selected "nanoparticle 1" (Fig. 3(a)) and "nanoparticle 2" (Fig. 3(d)). The integrated radial profiles of FFTs are shown on Fig. 3(g). It is clearly seen that "particle 1" is composed of 3C-Ag while the "particle 2" has the 4H-Ag structure.

Such a hexagonal structure of silver nanocrystals can be dictated by the arrangement of sulfur atoms on the surface of the outer WS_2 layer. Generally speaking, an arrangement of atoms in a sulfur layer in the S-W-S "sandwich" can be a perfect template for the growth of hexagonal close-packed (*hcp*) Ag atomic layers. Indeed, sulfur atoms of the WS_2 surface form a hexagonal array with a characteristic distance between the atoms of 3.15 Å. At the same time, the inter-atom distance in *hcp* Ag layer is about 2.9 Å (Fig. 3h). These *hcp* layers can be either

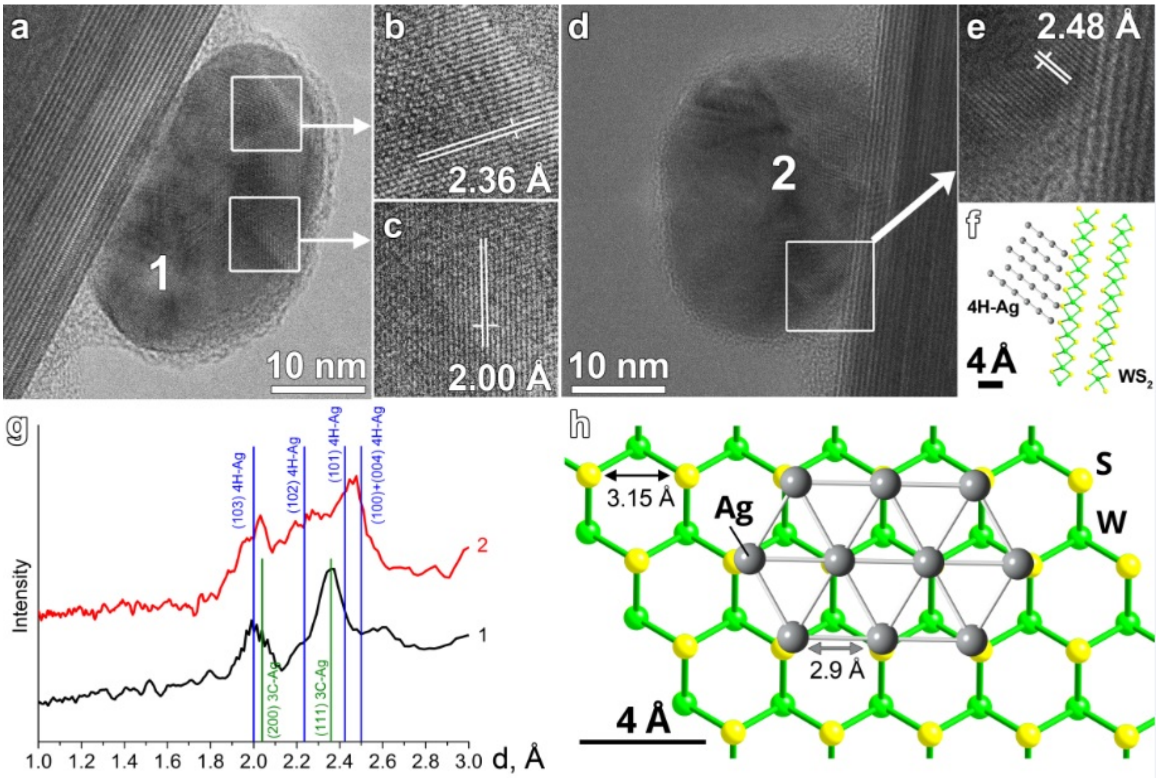

FIG. 3. (a-e) are HRTEM micrographs of AgNPs grown on the surface of NT-WS_2. (f) is a suggested crystallographic model for (e) in which (004) 4H-Ag planes continue the "chevrons" of outer WS_2 layers. (g) represents integrated radial profiles of FFTs calculated from nanoparticles 1 and 2 marked on (a) and (d), respectively. Data for 3C-Ag and 4H-Ag cells are taken from entries #4-783 and #41-1402 from ICDD PDF2 database [38]. The cif-files for crystallographic visualizations were taken from CrystalMaker Materials Library [43] and from the works [39, 44] using Crystallography Open Database [45]. (h) depicts the suggested model of *hcp* atomic silver layers grown on the surface of WS_2. Please, refer to the article text for more details

(111) planes of cubic silver (3C-Ag) or (004) planes of hexagonal silver (4H-Ag). If the silver *hcp* layers propagate parallel to the surface of NT-WS_2, their spacing will not be influenced by the disulfide substrate. However, if the silver hcp planes propagate nearly perpendicularly to the disulfide surface, 4H structure becomes more preferable. Sulfur atomic rows on the WS_2 surface are located at 2.73 Å distances, so a 4H-Ag with 2.50 Å spacing between hcp Ag layers matches better with those rows than the 3C-Ag with a 2.35 Å spacing of equivalent atomic planes. In this case, a sulfur atoms arrangement of NT-WS_2 can pre-organize the 4H-Ag motifs. This also can explain the observation of (004) 4H-Ag planes continuing the "chevrons" of outer WS_2 layer (Fig. 3(e,f)). It should be noted that 4H-polytype was initially observed in natural silver samples from northern USSR [39] and later in a number of synthetic nanostructures: AgNPs prepared using *Rumex hymenosepalus* extracts [40], silver nanowires [41] and thin films [42].

Of great importance is the fact that Ag-NT-WS_2 preparation by the proposed techniques does not require any additional reducing agents or linkers, thus providing nanocomposite synthesis a material efficiency. Within the first technique, the spontaneous reaction of $AgNO_3$ with WS_2 takes place, resulting in heterogeneous silver nucleation. Obviously, the driving force of such chemical interaction originates from the energy difference of WS_2 Fermi level and the redox potential of dissolved Ag^+ ions. The Fermi level of WS_2 is known to be of 4.7 range below the vacuum level [46]. The standard redox potential of Ag^+ ions is +0.799 V against the standard hydrogen electrode (SHE) [47]. The absolute potential of SHE is, in turn, reported to be within the -4.73 to -4.43 V range [48]. Thus, the Fermi level of tungsten disulfide should be higher by 0.5–0.8 eV than the energy of missed valence electron in Ag^+ ions (Fig. 4). This should result in spontaneous electron transfer from the NT-WS_2 surface to silver ions resulting in $Ag^+ \rightarrow Ag^0$ reduction and nucleation of silver nanocrystals. Obviously, the first Ag atoms became bound by surface sulfur atoms, dictating hexagonal silver crystal symmetry as described above. The electron deficiency in the nanotubes can further be compensated by WS_2 oxidation, e.g. at the nearest surface defects. $[Ag(NH_3)_2]OH$ has ca. twice lower reduction potential (+0.38 V) [47] then Ag^+, so the energy difference with WS_2 Fermi level is lower but still negative. However at 100 °C, the diamminesilver(I) complex decomposes rapidly initiating silver nucleation as described in [36]. Previously, it was shown that the presence of excessive ammonia in the reaction mixture can prevent secondary nucleation during citrate-mediated AgNP synthesis, leading to the formation of smaller and quasi-monodisperse nanoparticles [49]. This was explained by the entrapment of residual free Ag^+ ions responsible for secondary nucleation. Possibly, the same moderating effect of ammonia leads to the aforementioned formation of smaller AgNPs on NT-WS_2 when $[Ag(NH_3)_2]OH$ is employed instead of $AgNO_3$.

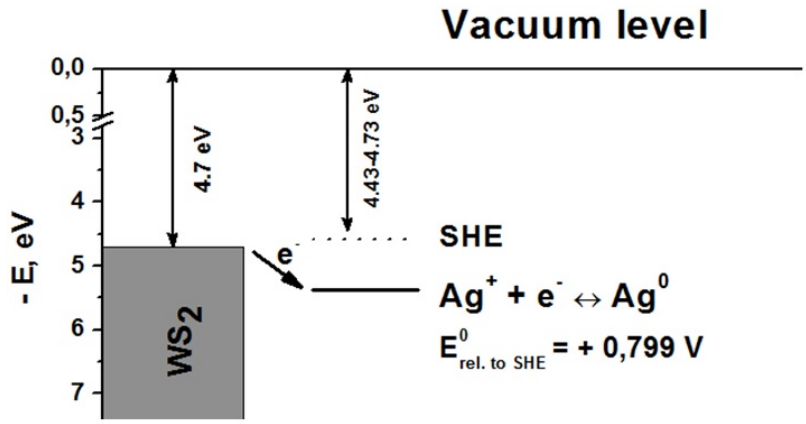

FIG. 4. Proposed energy diagram representing relative energies of WS_2 Fermy level and energy of missed valent electron in Ag^+ ion. The arrow designates possible electron transfer from NT-WS_2 to Ag^+ ions resulting in spontaneous AgNP growth on the sidewall of disulfide nanotubes

4. Conclusions

Reactions of aqueous $AgNO_3$ or $[Ag(NH_3)_2]OH$ solutions with NT-WS_2 resulted in functionalization of the nanotubes with a 5–60 nm layer of AgNPs without requiring any additional reducing agents. The spontaneous formation of AgNPs on NT-WS_2 surface is suggested to be driven by electron transfer from disulfide surface to dissolved Ag^I ions. Part of the grown AgNPs exhibited unusual hexagonal crystal structure (4H–Ag). Based on careful HRTEM study, the hexagonal arrangement of sulfur atoms within the WS_2 layers, including the outer disulfide layer, is suggested to predict the observed formation of 4H–Ag nanocrystals. The prepared nanocomposites may have applications as sensors or antibacterial low-friction surface coatings.

Acknowledgements

This work is supported by the Russian Science Foundation (grant 14-13-00871), AYP acknowledges partial personal support by the Russian Foundation for Basic Research (project # 16-33-01058 mol_a) and Lomonosov Moscow State University Program of Development (the use of Carl Zeiss Libra 200 MC microscope). Authors thank Maria Poliakova (Tsukuba University, Japan) for the proof-reading.

References

[1] Yang J., Liu H. *Metal-based composite nanomaterials*. Springer International Publishing, Cham, 2015, 259 p.
[2] Chin K.C., Gohel A., Chen W.Z., Elim H.I., Ji W., Chong G.L., Sow C.H., Wee A.T.S. Gold and silver coated carbon nanotubes: An improved broad-band optical limiter. *Chem. Phys. Lett.*, 2005, **409** (1–3), P. 85–88.
[3] Zhang J., Zhang X., Lai C., Zhou H., Zhu Y. Silver-decorated aligned CNT arrays as SERS substrates by high temperature annealing. *Optics Express*, 2014, **22**(18), P. 21157–21166.
[4] Sanles-Sobrido M., Rodríguez-Lorenzo L., Lorenzo-Abalde S., González-Fernández Á., Correa-Duarte M.A., Alvarez-Puebla R.A., Liz-Marzán L.M. Label-free SERS detection of relevant bioanalytes on silver-coated carbon nanotubes: The case of cocaine. *Nanoscale*, 2009, **1**(1), P. 153–158.
[5] Chen Y.-C., Young R.J., Macpherson J. V., Wilson N.R. Silver-decorated carbon nanotube networks as SERS substrates. *J. Raman Spectrosc.*, 2011, **42**(6), P. 1255–1262.
[6] Chang W.-T., Hsueh Y.-C., Huang S.-H., Liu K.-I., Kei C.-C., Perng T.-P., Lin C., Chen Z. Fabrication of Ag-loaded multi-walled TiO_2 nanotube arrays and their photocatalytic activity. *J. Mater. Chem. A*, The Royal Society of Chemistry, 2013, **1**(6), P. 1987–1991.

[7] Wu F., Hu X., Fan J., Liu E., Sun T., Kang L., Hou W., Zhu C., Liu H. Photocatalytic Activity of Ag/TiO_2 Nanotube Arrays Enhanced by Surface Plasmon Resonance and Application in Hydrogen Evolution by Water Splitting. *Plasmonics*, 2013, **8**(2), P. 501–508.

[8] Yan Y., Sun H., Yao P., Kang S.-Z., Mu J. Effect of multi-walled carbon nanotubes loaded with Ag nanoparticles on the photocatalytic degradation of rhodamine B under visible light irradiation. *Appl. Surf. Sci.*, 2011, **257**(8), P. 3620–3626.

[9] Liu W., Feng Y., Tang H., Yuan H., He S., Miao S. Immobilization of silver nanocrystals on carbon nanotubes using ultra-thin molybdenum sulfide sacrificial layers for antibacterial photocatalysis in visible light. *Carbon*, 2016, **96**, P. 303–310.

[10] Cui S., Pu H., Mattson E.C., Lu G., Mao S., Weinert M., Hirschmugl C.J., Gajdardziska-Josifovska M., Chen J. Ag nanocrystal as a promoter for carbon nanotube-based room-temperature gas sensors. *Nanoscale*, The Royal Society of Chemistry, 2012, **4**(19), P. 5887–5894.

[11] Cui S., Pu H., Lu G., Wen Z., Mattson E.C., Hirschmugl C., Gajdardziska-Josifovska M., Weinert M., Chen J. Fast and Selective Room-Temperature Ammonia Sensors Using Silver Nanocrystal-Functionalized Carbon Nanotubes. *ACS Appl. Mater. Interfaces*, 2012, **4**(9), P. 4898–4904.

[12] Liu Y., Wu G., Cui Y. Ag/CNT-catalyzed hydroamination of activated alkynes with aromatic amines. *Appl. Organomet. Chem.*, 2013, **27**(4), P. 206–208.

[13] Seo Y., Hwang J., Kim J., Jeong Y., Hwang M.P., Choi J. Antibacterial activity and cytotoxicity of multi-walled carbon nanotubes decorated with silver nanoparticles. *Int. J. Nanomedicine*, 2014, **9**, P. 4621–4629.

[14] Dinh N.X., Quy N. Van, Huy T.Q., Le A.-T. Decoration of Silver Nanoparticles on Multiwalled Carbon Nanotubes: Antibacterial Mechanism and Ultrastructural Analysis. *J. Nanomater.*, 2015, **2015**, P. 1–11.

[15] García B.O., Kharissova O.V., Rasika Dias H.V., Aguirre T. F.S., Hernández J.S. Nanocomposites with antibacterial properties using CNTs with magnetic nanoparticles. *Nanosyst. Physics, Chem. Math.*, 2016, **7**(1), P. 161–168.

[16] Castle A.B., Gracia-Espino E., Nieto-Delgado C., Terrones H., Terrones M., Hussain S. Hydroxyl-Functionalized and N-Doped Multiwalled Carbon Nanotubes Decorated with Silver Nanoparticles Preserve Cellular Function. *ACS Nano*, 2011, **5** (4), P. 2458–2466.

[17] Tenne R. Inorganic nanotubes and fullerene-like nanoparticles. *J. Mater. Res.*, 2006, **21**(11), P. 2726–2743.

[18] Margolin A., Rosentsveig R., Albu-Yaron A., Popovitz-Biro R., Tenne R. Study of the growth mechanism of WS2 nanotubes produced by a fluidized bed reactor. *J. Mater. Chem.*, 2004, **14**(4), P. 617–624.

[19] Višic B., Panchakarla L.S., Tenne R. Inorganic Nanotubes and Fullerene-like Nanoparticles at the Crossroads between Solid-State Chemistry and Nanotechnology. *J. Am. Chem. Soc.*, 2017, **139**(37), P. 12865–12878.

[20] Divon Y., Levi R., Garel J., Golberg D., Tenne R., Ya'akobovitz A., Joselevich E. Torsional Resonators Based on Inorganic Nanotubes. *Nano Lett.*, 2017, **17**(1), P. 28–35.

[21] Qin F., Shi W., Ideue T., Yoshida M., Zak A., Tenne R., Kikitsu T., Inoue D., Hashizume D., Iwasa Y. Superconductivity in a chiral nanotube. *Nat. Commun.*, 2017, **8**, P. 14465.

[22] Tsverin Y., Popovitz-Biro R., Feldman Y., Tenne R., Komarneni M.R., Yu Z., Chakradhar A., Sand A., Burghaus U. Synthesis and characterization of WS2 nanotube supported cobalt catalyst for hydrodesulfurization. *Mater. Res. Bull.*, 2012, **47**(7), P. 1653–1660.

[23] Komarneni M.R., Yu Z., Burghaus U., Tsverin Y., Zak A., Feldman Y., Tenne R. Characterization of Ni-Coated WS_2 Nanotubes for Hydrodesulfurization Catalysis. *Isr. J. Chem.*, 2012, **52**(11–12), P. 1053–1062.

[24] Tsverin Y., Livneh T., Rosentsveig R., Zak A., Pinkas I., Tenne R. Photocatalysis with hybrid Co-coated WS_2 nanotubes. *Nanomater. Energy*, 2013, **2**(1), P. 25–34.

[25] Višic B., Cohen H., Popovitz-Biro R., Tenne R., Sokolov V.I., Abramova N. V., Buyanovskaya A.G., Dzvonkovskii S.L., Lependina O.L. Direct Synthesis of Palladium Catalyst on Supporting WS_2 Nanotubes and its Reactivity in Cross-Coupling Reactions. *Chem. - An Asian J.*, 2015, **10**(10), P. 2234–2239.

[26] Sedova A., Leitus G., Feldman Y., Bendikov T., Popovitz-Biro R., Khodorov S., Dodiuk H., Kenig S., Tenne R. Synthesis of magnetic $FeWO_4$ nanoparticles and their decoration of WS2 nanotubes surface. *J. Mater. Sci.*, 2017, **52**(11), P. 6376–6387.

[27] Ksenevich V.K., Gorbachuk N.I., Viet H., Shuba M.V., Kuzhir P.P., Maksimenko S.A., Paddubskaya A.G., Valusis G., Wieck A.D., Zak A., Tenne R. Electrical properties of carbon nanotubes/WS_2 nanotubes (nanoparticles) hybrid films. *Nanosyst. Physics, Chem. Math.*, 2016, **7**(1), P. 37–43.

[28] Daoush W.M., Hong S.H. Synthesis of multi-walled carbon nanotube/silver nanocomposite powders by chemical reduction in aqueous solution. *J. Exp. Nanosci.*, 2013, **8**(5), P. 742–751.

[29] Yamada T., Hayashi Y., Takizawa H. Synthesis of Carbon Nanotube/Silver Nanocomposites by Ultrasonication. *Mater. Trans.*, 2010, **51**(10), P. 1769–1772.

[30] Maley J., Schatte G., Yang J., Sammynaiken R. Spontaneous Ag-Nanoparticle Growth at Single-Walled Carbon Nanotube Defect Sites: A Tool for *In Situ* Generation of SERS Substrate. *J. Nanotechnol.*, 2011, **2011**, P. 1–7.

[31] Shahar C., Levi R., Cohen S.R., Tenne R. Gold Nanoparticles as Surface Defect Probes for WS 2 Nanostructures. *J. Phys. Chem. Lett.*, 2010, **1**(2), P. 540–543.

[32] Polyakov A.Y., Yadgarov L., Popovitz-Biro R., Lebedev V.A., Pinkas I., Rosentsveig R., Feldman Y., Goldt A.E., Goodilin E.A., Tenne R. Decoration of WS_2 nanotubes and fullerene-like MoS_2 with gold nanoparticles. *J. Phys. Chem. C*, 2014, **118**(4), P. 2161–2169.

[33] Polyakov A.Y., Nesterov A. V, Goldt A.E., Zubyuk V., Dolgova T., Yadgarov L., Visic B., Fedyanin A.A., Tenne R., Goodilin E.A. Optical properties of multilayer films of nanocomposites based on WS_2 nanotubes decorated with gold nanoparticles. *J. Phys. Conf. Ser.*, 2015, **643**, P. 012046.

[34] Tremel W., Spetter D., Hoshyargar F., Sahoo J., Tahir M.N., Branscheid R., Barton B., Panthöfer M., Kolb U. Surface Defects as a Tool to Solubilize and Functionalize WS2 Nanotubes. *Eur. J. Inorg. Chem.*, 2017, **15**, P. 2190–2194.

[35] Zak A., Ecker L.S., Efrati R., Drangai L., Fleischer N., Tenne R. Large-scale Synthesis of WS2 Multiwall Nanotubes and their Dispersion, an Update. *J. Sensors Transducers*, 2011, **12** (Special Issue), P. 1–10.

[36] Sarycheva A.S., Ivanov V.K., Baranchikov A.E., Savilov S. V., Sidorov A. V., Goodilin E.A., Grigorieva A. V., Maksimov G. V., Goodilin E.A., Egorov A. V., Brazhe A.R., Parshina E.Y., Luneva O.G., Maksimov G. V., Tretyakov Y.D. Microbead silica decorated with polyhedral silver nanoparticles as a versatile component of sacrificial gel films for SERS applications. *RSC Adv.*, 2015, **5**(110), P. 90335–90342.

[37] Neas D., Klapetek P. Gwyddion: an open-source software for SPM data analysis. *Open Phys.*, 2012, **10**(1), P. 181–188.

[38] ICDD Products - PDF-2 [Electronic resource], URL: http://www.icdd.com/products/pdf2.htm (accessed: 06.10.2017).

[39] Novgorodova M.I., Gorshkov A.I., Mokhov A. V. Native Silver and Its New Structural Modifications. *Zap. Vsesoyuznogo Mineral. Obs.*, 1979, **108**, P. 552–563.

[40] Rodríguez-León E., Iñiguez-Palomares R., Navarro R., Herrera-Urbina R., Tánori J., Iñiguez-Palomares C., Maldonado A. Synthesis of silver nanoparticles using reducing agents obtained from natural sources (*Rumex hymenosepalus* extracts). *Nanoscale Res. Lett.*, 2013, **8**(1), P. 318.

[41] Liu X., Luo J., Zhu J. Size effect on the crystal structure of silver nanowires. *Nano Lett.*, 2006, **6**(3), P. 408–412.

[42] Chakraborty I., Shirodkar S.N., Gohil S., Waghmare U. V, Ayyub P. A stable, quasi-2D modification of silver: optical, electronic, vibrational and mechanical properties, and first principles calculations. *J. Phys. Condens. Matter*, 2014, **26**(2), P. 25402.

[43] CrystalMaker Structures Libraries: Materials Strutures [Electronic resource], URL: http://crystalmaker.com/library/chalcogenides.html (accessed: 06.10.2017).

[44] Jette E.R., Foote F. Precision Determination of Lattice Constants. *J. Chem. Phys.*, 1935, **3**(10), P. 605–616.

[45] Crystallography Open Database [Electronic resource], URL: http://www.crystallography.net/cod/index.php (accessed: 05.10.2017).

[46] Jaegermann W., Ohuchi F.S., Parkinson B.A. Interaction of Cu, Ag and Au with van der Waals faces of WS_2, and SnS_2. *Surf. Sci.*, 1988, **201**(1–2), P. 211–227.

[47] Goia D. V., Matijević E. Preparation of monodispersed metal particles. *New J. Chem.*, 1998, **22** (11), P. 1203–1215.

[48] Reiss H., Heller A. The absolute potential of the standard hydrogen electrode: a new estimate. *J. Phys. Chem.*, 1985, **89**(20), P. 4207–4213.

[49] Gorup L.F., Longo E., Leite E.R., Camargo E.R. Moderating effect of ammonia on particle growth and stability of quasi-monodisperse silver nanoparticles synthesized by the Turkevich method. *J. Colloid Interface Sci.*, 2011, **360**(2), P. 355–358.